

# Linear waves in two-layer fluids over periodic bottoms

Jie Yu<sup>1,†</sup> and Leo R. M. Maas<sup>2,3</sup>

<sup>1</sup>Department of Civil Engineering, and School of Marine and Atmospheric Sciences,  
Stony Brook University, Stony Brook, NY 11794, USA

<sup>2</sup>Royal Netherlands Institute for Sea Research, PO Box 59, 1790 AB Texel, The Netherlands

<sup>3</sup>Institute for Marine and Atmospheric Research Utrecht, Utrecht University, Princetonplein 5,  
3584 CC, The Netherlands

(Received 24 July 2015; revised 18 January 2016; accepted 11 March 2016;  
first published online 6 April 2016)

A new, exact Floquet theory is presented for linear waves in two-layer fluids over a periodic bottom of arbitrary shape and amplitude. A method of conformal transformation is adapted. The solutions are given, in essentially analytical form, for the dispersion relation between wave frequency and generalized wavenumber (Floquet exponent), and for the waveforms of free wave modes. These are the analogues of the classical Lamb's solutions for two-layer fluids over a flat bottom. For internal modes the interfacial wave shows rapid modulation at the scale of its own wavelength that is comparable to the bottom wavelength, whereas for surface modes it becomes a long wave carrier for modulating short waves of the bottom wavelength. The approximation using a rigid lid is given. Sample calculations are shown, including the solutions that are inside the forbidden bands (i.e. Bragg resonated).

**Key words:** geophysical and geological flows, internal waves, stratified flows

## 1. Introduction

Wave propagation over a bottom topography is a mathematically challenging problem, from small-scale, free-surface waves to large-scale waves in geophysical fluids (Rhines & Bretherton 1973; Athanassoulis & Belibassakis 1999). Even with the restriction to linear dynamics, there are few exact analytical solutions but a broad range of approximated theories, most of which exploit the inhomogeneities of the medium by considering gentle slopes, small amplitudes or abrupt changes in bottom topographies. The complexity and difficulty in this type of problems arise in the intermediate case, where wavelength, depth and bottom variations have comparable scales, making the inhomogeneity of the medium neither gradual nor small nor localized (Rhines & Bretherton 1973; Weidman *et al.* 2015).

In a series of papers (Howard & Yu 2007; Yu & Howard 2010, 2012), a new and general treatment has been developed for linear free-surface water waves over arbitrary periodic topographies. The success of the theory rests on two principal ideas: the construction of an analytical conformal map that transforms the flow

† Email address for correspondence: [Jie.Yu.1@stonybrook.edu](mailto:Jie.Yu.1@stonybrook.edu)

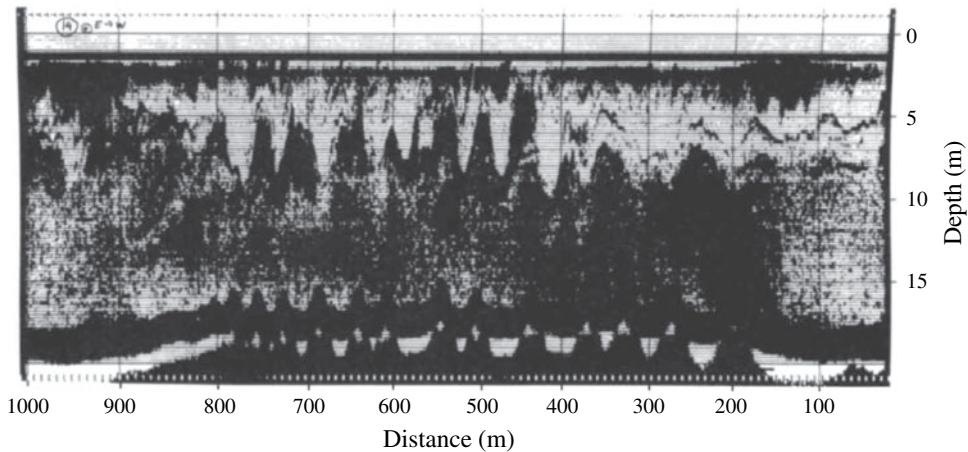


FIGURE 1. Acoustic image showing the internal waves trapped over a series of approximately periodic bottom ridges in the Rotterdam Waterway, The Netherlands. The internal wave wavelengths are comparable to that of the topography generating them. The largest internal wave height is approximately three to four times that of the topography. Image reproduced from Pietrzak *et al.* (1990) with the copyright permission from Nature.

domain onto a uniform strip, and the use of Floquet theory to exploit the spatial periodicity. The theory provides a set of exact linear modes for periodic bottoms that is analogous to the set of propagating and evanescent waves on a horizontal flat bed, becoming the second known complete basis for water waves. Applications have been made, demonstrating that this set of Floquet modes can indeed be used to construct solutions to various boundary value problems involving finite domains of an undulating bottom (Yu & Zheng 2012; Weidman *et al.* 2015).

In this paper, we adapt these ideas to the case of two layers of fluids over periodic bottoms, focusing on the free wave modes. In stratified fluids, internal wave motion is an important and ubiquitous component of the dynamics, having strong influence on the transport and mixing of mass and momentum, with important implications for chemical, biological and sediment processes in such systems. In coastal oceans and estuaries, internal waves generated by, and interacting with, topographies and boundaries are of particular interest. While many studies focus on isolated topographic features, observations show that there are resonant internal waves over nearly periodic bottoms (Pietrzak, Kranenburg & Abraham 1990; Pietrzak and Labeur 2004); see figure 1.

The present study offers a first step towards addressing the impact of bottom topography on both surface, as well as internal, wave modes allowed by a two-layer system. For this, a finite-amplitude, periodic bottom, fully submerged in the lower layer, is considered here. The theory is valid for any given frequency, therefore allowing spatially varying solutions at both slow and fast scales, meaning that exactly or quasi-spatially periodic, as well as unstable, resonant waves can all be found. These solutions show the bottom scale expressed in the interfacial displacements of the internal and surface wave modes. (In this paper, we shall refer to the solutions of the Laplace equation and top and bottom boundary conditions as the ‘modes’ or ‘wave modes’. For each mode, the displacements of the upper (free) and lower (interfacial) surface are synonymously referred to as the waves.)

The resonant waves mentioned above are analogous to the phenomenon of Bragg reflections, also called Bragg scattering or Bragg resonances, encountered in X-ray diffraction in crystals. When the wave frequency falls into a resonance band, the amplitude of the wave varies exponentially in space. These waves cannot exist in an open domain of continuous periodic bottom. Thus, these frequency bands are referred to as the ‘forbidden bands’ in physics. For water waves, resonant reflections can be well illustrated by considering a linear surface wave incident upon a series of submerged small sandbars in an otherwise flat seabed. Each bar crest can cause a little bit of reflection, individually negligible. However, if the incident wave has a frequency such that its wavelength is close to two times the bar spacing, reflections from successive crests are in phase and add up to form a strong reflected wave at the seaward side of the bar field. Due to energy losses to the back-scattered waves, the incident wave amplitude decreases shorewards over the bar field. This is the primary Bragg reflection. In general, resonant reflections occur when an integer number of incident wavelengths  $\lambda$  is close to twice the bottom wavelength  $\lambda_{bed}$ , i.e.  $\lambda \simeq (2/m)\lambda_{bed}$ ,  $m = 1, 2, \dots$  (Yu & Howard 2010). Bragg scattering of water waves by a patch of periodic bed has been extensively studied in the literature, including a recent perturbation analysis for two-layer fluids over small-amplitude bottom corrugations (Alam, Liu & Yue 2009). In such wave scattering problems, the focus is typically on the amplitudes of the reflected and transmitted waves (with respect to that of the incident wave arriving at the bar patch).

Although it gives the solutions for resonant frequencies, the present work is fundamentally different from those studies of wave scattering by a patch of periodic seabed, nor do we necessarily want to restrict ourselves to any particular frequencies. Here, we consider a periodic bed extending continuously in a domain of indefinite length. The question of interest to us is the dispersion relationship determining the spatial scales (i.e. the eigenvalues or wavenumber equivalent) of the motion for a given temporal frequency and the corresponding solutions (eigenfunctions) of the flow field. For a generally periodic bed, these are the analogues of Lamb’s (1932) solutions for a two-layer fluid over a flat bed. For such eigenmodes, reflection and transmission are irrelevant (as the domain of periodic bed is indefinitely long and there is no preference of an incident wave to scattered wave). However, such eigenmodes can be used to formulate the boundary value problems of wave scattering in a domain with a finite extent of bottom corrugations, as e.g. in Yu & Zheng (2012) for one-layer fluids.

Another difference that should be emphasized is the classification and interpretation of Bragg reflections. In their perturbation analysis, Alam *et al.* (2009) interpreted the resonances using the classical wave–wave interaction theory by treating the bottom (which is fixed) as a wave with zero frequency, following the framework of Liu & Yue (1998) in the case of one-layer fluids, and referred to such as ‘nonlinear resonant interaction’. Although different classes of resonant waves are resolved at different orders of the perturbation analysis, the forcing mechanisms are primarily due to the linear dynamics of the wave motion interacting with the bottom. This is particularly clear from the evolution equations for the so-called Class I and II resonances in Alam *et al.* (2009). As is pointed out in Yu & Howard (2010), Bragg reflection is fundamentally a linear wave phenomenon, and does not necessarily follow the framework of nonlinear wave–wave interaction. Indeed, Yu & Howard (2010) showed that both primary- and higher-order resonances (referring to the original classification in X-ray work) can be solved and interpreted using linear theory. This is similarly seen here for the resonant interfacial waves. Of course, nonlinear convective inertia can raise interesting effects, but can be addressed separately.

The rest of the paper is organised as follows. In § 2 the mathematical formulation is presented, arriving at a determinantal equation for the dispersion relation between the frequency and Floquet exponent (which is related to the wavenumber). Calculations of the dispersion relation are given in § 3, including the comparison with Lamb's equation for a flat bottom. Waveforms for both internal and surface modes are shown and discussed in § 4, including the cases when the frequencies are Bragg resonant. Challenges in future research to extend and apply the present theory are discussed in § 5.

## 2. Formulation

Consider two layers of inviscid incompressible fluids over a periodic bottom. Let  $z$  point upwards and  $z=0$  be the undisturbed interface. The bottom is at  $z=-H_\ell+H_b(x)$ , where  $H_\ell$  is the mean (undisturbed) thickness of the lower-layer fluid of density  $\rho_\ell$  and  $H_b(x)$  is the periodic bed profile. In this study, we shall only consider the case where  $H_b(x)$  is submerged in the lower-layer fluid. The undisturbed free surface is at  $z=H_u$ , i.e.  $H_u$  is the thickness of the upper-layer fluid of density  $\rho_u < \rho_\ell$ . For small displacements of the free surface and interface (but not necessarily small amplitude of bottom undulations), the linearized equations for the velocity potentials  $\phi_u$  and  $\phi_\ell$  are written, as follows. For the upper-layer fluid,

$$\nabla^2 \phi_u = 0 \quad \text{for } 0 < z < H_u, \quad (2.1)$$

$$\phi_{u,tt} + g\phi_{u,z} = 0 \quad \text{at } z = H_u, \quad (2.2)$$

where  $x, z, t$  subscripts denote partial derivatives and  $g$  is the gravity. For the lower-layer fluid,

$$\nabla^2 \phi_\ell = 0 \quad \text{for } -H_\ell + H_b(x) < z < 0, \quad (2.3)$$

$$\phi_{\ell,x} H_{b,x} = \phi_{\ell,z} \quad \text{at } z = -H_\ell + H_b(x). \quad (2.4)$$

At the interface, the continuity of pressure and normal velocity lead to

$$\phi_{u,tt} + g(1-R)\phi_{u,z} = R\phi_{\ell,tt} \quad \text{at } z = 0, \quad (2.5)$$

$$\zeta_{\ell,t} = \phi_{\ell,z} = \phi_{u,z} \quad \text{at } z = 0, \quad (2.6)$$

where  $R = \rho_\ell/\rho_u > 1$  and  $\zeta_\ell$  is the displacement of the interface. Similarly, the displacement of the free surface is denoted by  $\zeta_u$  and satisfies

$$\zeta_{u,t} = \phi_{u,z} \quad \text{at } z = H_u. \quad (2.7)$$

Let  $\lambda_{bed}$  be the spatial period of the seabed profile  $H_b(x)$ . We shall normalize the problem to be  $\pi$ -periodic, following the practice in Mathieu's equation to which the general idea of Floquet solutions applies (Yu & Howard 2012). For this purpose, we define a wavenumber

$$k_B = \pi/\lambda_{bed}, \quad (2.8)$$

which corresponds to a wavelength  $2\lambda_{bed}$ . Denoting dimensionless variables by primes, we choose the following normalization.

$$\left. \begin{aligned} x' &= k_B x, & z' &= k_B z, & t' &= t\sqrt{gk_B}, \\ (\zeta'_\ell, \zeta'_u) &= (\zeta_\ell, \zeta_u)/a, & (\phi'_\ell, \phi'_u) &= (\phi_\ell, \phi_u)k_B/(a\sqrt{gk_B}), \end{aligned} \right\} \quad (2.9)$$

where  $a$  characterizes the interfacial wave amplitude, and is assumed to be infinitesimal for linear waves. The normalized (mean) depths and bottom profile are,

$$h'_u = k_B H_u, \quad h'_\ell = k_B H_\ell, \quad h'_b(x') = k_B H_b(x). \quad (2.10a-c)$$

For time-periodic solutions,

$$(\phi'_\ell, \phi'_u, \zeta'_\ell, \zeta'_u) = \left( \widehat{\phi}'_\ell(x, z), \widehat{\phi}'_u(x, z), \widehat{\zeta}'_\ell(x), \widehat{\zeta}'_u(x) \right) e^{-i\sigma t'} + \text{c.c.}, \quad (2.11)$$

where

$$\sigma = \omega / \sqrt{gk_B} \quad (2.12)$$

is the dimensionless frequency. Dropping the primes for clarity, from (2.1)–(2.5) the dimensionless equations for the amplitudes of solutions are written as follows. For the upper-layer fluid,

$$\nabla^2 \widehat{\phi}_u = 0 \quad \text{for } 0 < z < h_u, \quad (2.13)$$

$$-\sigma^2 \widehat{\phi}_u + \widehat{\phi}_{u,z} = 0 \quad \text{at } z = h_u. \quad (2.14)$$

For the lower-layer fluid,

$$\nabla^2 \widehat{\phi}_\ell = 0 \quad \text{for } -h_\ell + h_b(x) < z < 0, \quad (2.15)$$

$$\widehat{\phi}_{\ell,x} h_{b,x} = \widehat{\phi}_{\ell,z} \quad \text{at } z = -h_\ell + h_b(x). \quad (2.16)$$

At the interface,

$$-\sigma^2 \widehat{\phi}_u + (1 - R) \widehat{\phi}_{u,z} = -\sigma^2 R \widehat{\phi}_\ell \quad \text{at } z = 0. \quad (2.17)$$

$$-i\sigma \widehat{\zeta}_\ell = \widehat{\phi}_{\ell,z} = \widehat{\phi}_{u,z} \quad \text{at } z = 0. \quad (2.18)$$

We shall note that the scaling implies that the nonlinear terms in the Euler equations are of  $O(ak_B)$  or smaller. So, the linear theory, requiring  $ak \ll 1$ , where  $k$  is the water wavenumber, is valid when  $k/k_B$  is small or finite. One might expect nonlinearity to become important for  $k/k_B \gg 1$ , but the waves are so short that the bottom becomes irrelevant, and thus the typical scaling  $ak$  should be restored.

### 2.1. The conformal transformation and the lower-layer problem

In view of the linearized matching conditions at the interface, (2.17) and (2.18), we shall apply a conformal transformation only to the lower-layer fluid domain in order to deal with the topography. In the mapped plane  $(\xi, \eta)$ , the bed  $z = -h_\ell + h_b(x)$  is transformed into a horizontal flat bottom  $\eta = -h$  and the undisturbed interface  $z = 0$  into  $\eta = 0$ . The transformation functions are

$$x = \xi - h \sum_{j=1}^{\infty} (b_j \sin 2j\xi - c_j \cos 2j\xi) \cosh 2j\eta / \sinh (2jh), \quad (2.19)$$

$$z = \eta - h \sum_{j=1}^{\infty} (b_j \cos 2j\xi + c_j \sin 2j\xi) \sinh 2j\eta / \sinh (2jh), \quad (2.20)$$

where the Fourier coefficients  $b_j$  and  $c_j$  are determined implicitly from

$$-h_\ell + h_b(x) = -h + h \sum_{j=1}^{\infty} (b_j \cos 2j\xi + c_j \sin 2j\xi), \quad (2.21)$$

$$x = \xi - h \sum_{j=1}^{\infty} (b_j \sin 2j\xi - c_j \cos 2j\xi) \coth(2jh), \quad (2.22)$$

as the result of requiring the corrugated seabed to be mapped onto  $\eta = -h$ . The transformation functions (2.19) and (2.20) imply that  $\xi$  and  $\eta$  are also normalized using  $k_B$ . We shall require  $h_b(x)$  to have zero spatial average in  $x$ , so that  $h_\ell$  is the mean depth of the lower layer. As a consequence of this, as well as the fact that the map preserves the spatial periodicity of the bottom (being periodic in both  $x$  and  $\xi$  with the same period  $\pi$ ), the water depth  $h$  in the mapped plane must be determined together with the coefficients  $b_j$  and  $c_j$ , thus finding the map. Averaging (2.21) over  $x$ , noting that  $dx = (dx/d\xi)d\xi$  with  $dx/d\xi$  obtained from (2.22), we have,

$$h_\ell = h + h^2 \sum_{j=1}^{\infty} (b_j^2 + c_j^2) j \coth(2jh). \quad (2.23)$$

It is clear that  $h < h_\ell$ . Mathematically this is due to the stretching of conformal mapping. From the physical point of view, it reflects the fact that the wave is more affected by the bed crests than by the troughs that are deeper down. Thus, the water depth ‘seen’ by the wave is shallower than the mean depth  $h_\ell$ , effectively being characterized by the depth  $h$  in the mapped plane. This is particularly noticeable when the bottom amplitude is large. Of course, the choice above is not unique. We could specify the depth in the mapped plane, but would then have to allow a non-zero spatial average of  $h_b(x)$ . We cannot over-specify the conditions on the transformation functions. For details of computing the map, the reader is referred to Yu & Howard (2012). From this point on, for a given bottom profile  $h_b(x)$ , we consider the map parameters  $b_j$ ,  $c_j$  and  $h$  to be known.

In the mapped plane, (2.15) and (2.16) become

$$\widehat{\phi}_{\ell,\xi\xi} + \widehat{\phi}_{\ell,\eta\eta} = 0 \quad \text{for } -h < \eta < 0, \quad (2.24)$$

$$\widehat{\phi}_{\ell,\eta} = 0 \quad \text{at } \eta = -h. \quad (2.25)$$

Following the Floquet theory for a one-layer fluid over a periodic bottom (Yu & Howard 2012), we write the solution in the form

$$\widehat{\phi}_\ell = e^{\mu\xi} P(\xi, \eta; \mu, \sigma), \quad (2.26)$$

where

$$P(\xi, \eta; \mu, \sigma) = \sum_{n=-\infty}^{\infty} D_n e^{in\xi} \frac{\cosh[(n - i\mu)(\eta + h)]}{\cosh[(n - i\mu)h]} \quad (2.27)$$

is the periodic factor corresponding to the Floquet exponent  $\mu$  for a given frequency  $\sigma$ . It is readily seen that this satisfies (2.24) and (2.25). The Floquet exponent  $\mu$  and the corresponding Fourier coefficients  $D_n$  are yet to be determined, by satisfying the conditions (2.17) and (2.18) at the interface.

To complete the matching conditions, cf. § 2.3, we need to obtain  $\widehat{\phi}_{\ell,z}|_{z=0}$ . Under the transformation,

$$\frac{\partial}{\partial z} = \xi_z \frac{\partial}{\partial \xi} + \eta_z \frac{\partial}{\partial \eta}. \quad (2.28)$$

Taking the derivative in  $z$ , and evaluating at  $z=0$  (i.e.  $\eta=0$ ), we get from (2.19) and (2.20)  $\xi_z=0$  and  $\eta_z=1/Q(\xi)$  at  $z=0$ , where

$$Q(\xi) = 1 - h \sum_{j=1}^{\infty} (b_j \cos 2j\xi + c_j \sin 2j\xi) 2j / \sinh(2jh) \quad (2.29)$$

is related to the Jacobian of transformation, i.e.  $J^{1/2} = Q(\xi)$  at  $z=0$ . Thus,

$$\widehat{\phi}_{\ell,z}|_{z=0} = Q^{-1} \widehat{\phi}_{\ell,\eta}|_{\eta=0}. \quad (2.30)$$

For later convenience, we quote here

$$\widehat{\phi}_{\ell}|_{z=0} = \sum_{n=-\infty}^{\infty} D_n e^{(\mu+in)\xi}, \quad (2.31)$$

$$\widehat{\phi}_{\ell,\eta}|_{z=0} = \sum_{n=-\infty}^{\infty} D_n e^{(\mu+in)\xi} Z_n(\mu), \quad (2.32)$$

where

$$Z_n(\mu) \equiv (n - i\mu) \tanh[(n - i\mu)h]. \quad (2.33)$$

Recall that at  $z=0$ ,  $x$  and  $\xi$  are related via (2.19), i.e.

$$x = \xi + f(\xi), \quad f(\xi) \equiv -h \sum_{j=1}^{\infty} (b_j \sin 2j\xi - c_j \cos 2j\xi) / \sinh(2jh). \quad (2.34)$$

## 2.2. The upper-layer problem

As can be verified by direct substitution, the solution that satisfies (2.13) and (2.14) can be written as

$$\begin{aligned} \widehat{\phi}_u &= \sum_{n=-\infty}^{\infty} e^{(\mu+in)x} \frac{B_n}{\cosh[(n - i\mu)h_u]} \\ &\times \left\{ \cosh[(n - i\mu)(z - h_u)] + \frac{\sigma^2}{(n - i\mu)} \sinh[(n - i\mu)(z - h_u)] \right\}. \end{aligned} \quad (2.35)$$

It must also satisfy the conditions at the interface (2.18) and (2.17). At  $z=0$ ,

$$\widehat{\phi}_{u,z} = \sum_{n=-\infty}^{\infty} e^{(\mu+in)x} B_n Y_n(\sigma, \mu), \quad (2.36)$$

where

$$Y_n(\sigma, \mu) \equiv \sigma^2 - (n - i\mu) \tanh[(n - i\mu)h_u], \quad (2.37)$$



and

$$-\sigma^2 \widehat{\phi}_u + (1-R) \widehat{\phi}_{u,z} = - \sum_{n=-\infty}^{\infty} e^{(\mu+in)x} B_n \sigma^2 L_n(\sigma, \mu), \quad (2.38)$$

where

$$L_n(\sigma, \mu) \equiv R - \left\{ \frac{\sigma^2}{(n-i\mu)} + (R-1) \frac{(n-i\mu)}{\sigma^2} \right\} \tanh[(n-i\mu)h_u]. \quad (2.39)$$

These will be needed to complete the matching conditions at  $z=0$ , as follows.

### 2.3. Matching at the interface and the dispersion relationship

The objective here is to convert  $e^{(\mu+in)\xi}$ , appearing in (2.31) and (2.32), into a Fourier series in  $x$ . It follows from (2.34),

$$e^{(\mu+in)\xi} = e^{(\mu+in)x} e^{-(\mu+in)f(\xi)}. \quad (2.40)$$

Since  $f(\xi)$  is  $\pi$ -periodic in  $\xi$ , hence so in  $x$ , the function  $e^{-(\mu+in)f(\xi)}$  is  $\pi$ -periodic in  $x$  and can be written in a Fourier series, i.e.

$$e^{-(\mu+in)f(\xi)} = \sum_{j=-\infty}^{\infty} A_{n,j} e^{i2jx}. \quad (2.41)$$

Since (2.34) depends on the known map parameters  $b_j$ ,  $c_j$  and  $h$ , we now consider  $A_{n,j}$  to be known. Applying an index shift, (2.31) and (2.32) can be rewritten as

$$\widehat{\phi}_\ell|_{\eta=0} = \sum_{n=-\infty}^{\infty} e^{(\mu+in)x} \sum_{j=-\infty}^{\infty} D_{n-2j} A_{n-2j,j}, \quad (2.42)$$

$$\widehat{\phi}_{\ell,\eta}|_{\eta=0} = \sum_{n=-\infty}^{\infty} e^{(\mu+in)x} \sum_{j=-\infty}^{\infty} D_{n-2j} A_{n-2j,j} Z_{n-2j}. \quad (2.43)$$

Similarly, the function  $Q(\xi)$  in (2.29) can be written as

$$Q(\xi) = \sum_{j=-\infty}^{\infty} Q_j e^{i2jx}, \quad (2.44)$$

where  $Q_0 \neq 0$  is real, and  $Q_j$  and  $Q_{-j}$  are complex conjugates. Note that the  $Q_j$ 's depend only on the map, hence the properties of bottom profile, being independent of  $\sigma$  and  $\mu$ .

Substituting (2.38) and (2.42) into (2.17), cancelling the common factor  $e^{\mu x}$  and collecting the coefficients of  $e^{inx}$ , we find

$$R \sum_{j=-\infty}^{\infty} D_{n-2j} A_{n-2j,j} = B_n L_n(\sigma, \mu). \quad (2.45)$$

In view of (2.30), we rewrite from (2.18)

$$\widehat{\phi}_{\ell,\eta} = Q \widehat{\phi}_{u,z} \quad \text{at } z=0. \quad (2.46)$$



Substituting in (2.36), (2.43) and (2.44), shifting the index and again cancelling the factor  $e^{\mu x}$ , we collect the coefficients of  $e^{inx}$ , obtaining

$$\sum_{j=-\infty}^{\infty} D_{n-2j} A_{n-2j,j} Z_{n-2j} = \sum_{j=-\infty}^{\infty} B_{n-2j} Q_j Y_{n-2j}. \quad (2.47)$$

Equations (2.45) and (2.47) form a homogenous system for determining  $D_n$  and  $B_n$ .

Define the column vectors

$$\mathbf{D} = [\cdots D_{-n} \cdots D_n \cdots], \quad \mathbf{B} = [\cdots B_{-n} \cdots B_n \cdots]. \quad (2.48a,b)$$

In matrix form, (2.45) and (2.47) can be rewritten as

$$\mathbf{M}_1 \mathbf{D} = \mathbf{M}_2 \mathbf{B}, \quad \mathbf{M}_3 \mathbf{D} = \mathbf{M}_4 \mathbf{B}. \quad (2.49a,b)$$

It is readily seen from (2.45) that  $\mathbf{M}_2$  is diagonal and invertible since the diagonal elements  $L_n(\sigma, \mu) \neq 0$ . (In an even- $n$  representation,  $L_0 = R - \sigma^2 h_u \neq 0$  for  $\mu = 0$ .) Thus, we rewrite from (2.49)

$$\mathbf{B} = \mathbf{M}_2^{-1} \mathbf{M}_1 \mathbf{D}, \quad (2.50)$$

$$\mathbf{M} \mathbf{D} = 0, \quad \text{where } \mathbf{M} = \mathbf{M}_3 - \mathbf{M}_4 \mathbf{M}_2^{-1} \mathbf{M}_1. \quad (2.51)$$

The determinant  $\det(\mathbf{M})$  is a function of  $\mu$  and  $\sigma$ , given the parameters  $h_\ell$ ,  $h_u$  and  $R$ , as well as the map parameters  $h$ ,  $b_j$  and  $c_j$  which represent the properties of the bottom profile. Let us denote  $\Delta(\mu, \sigma; h_\ell, h_u, R, \mathcal{B}) \equiv \det(\mathbf{M})$ , where  $\mathcal{B}$  collectively represents  $\{b_j, c_j, h\}$ . For a non-trivial solution  $D_n$ , we require

$$\Delta(\mu, \sigma; h_\ell, h_u, R, \mathcal{B}) = 0. \quad (2.52)$$

For spatial periodic motions, the Floquet exponent  $\mu$  is purely imaginary, together with the period of  $P(\xi, \eta; \mu, \sigma)$  determining the spatial periodicity. In other words, for general periodic bottoms, (2.52) is the analogue of the dispersion relationship for two-layer fluids over a flat bottom (Lamb 1932, article 231).

For some frequencies, (2.52) cannot be satisfied by purely imaginary  $\mu$ , but require real  $\mu$ ; thus spatially periodic motion does not exist. This is the case when Bragg resonances occur. Given the average depths  $h_u$  and  $h_\ell$ , density ratio  $R$  and bottom profile, these frequencies appear as isolated narrow bands, i.e. ‘forbidden bands’ (since, however small the real  $\mu$  is, the wave amplitudes will become spatially unbounded in either positive or negative  $x$  direction, unless the flow domain is finite).

We note that  $\mu$  and  $-\mu$  are both solutions of (2.52) for the given frequency  $\sigma$ . The sign signifies the direction of wave propagation in the case of purely imaginary  $\mu$ , and the direction of spatial growth of wave amplitude in the case of real  $\mu$ .

### 3. Calculation of the dispersion relation

Finding the roots of (2.52) can be done, e.g. by using MatLab. Since we are only interested in the zeros of the determinant, we can scale the rows and columns by positive constants to improve the condition of the infinite matrix  $\mathbf{M}$  (Yu & Howard 2012). Let  $\Delta h_b$  be the crest-to-trough height of bottom profile  $h_b(x)$ . When  $\Delta h_b = 0$ , (2.52) reduces to Lamb’s dispersion relation for a flat bottom; see appendix A. Lamb’s

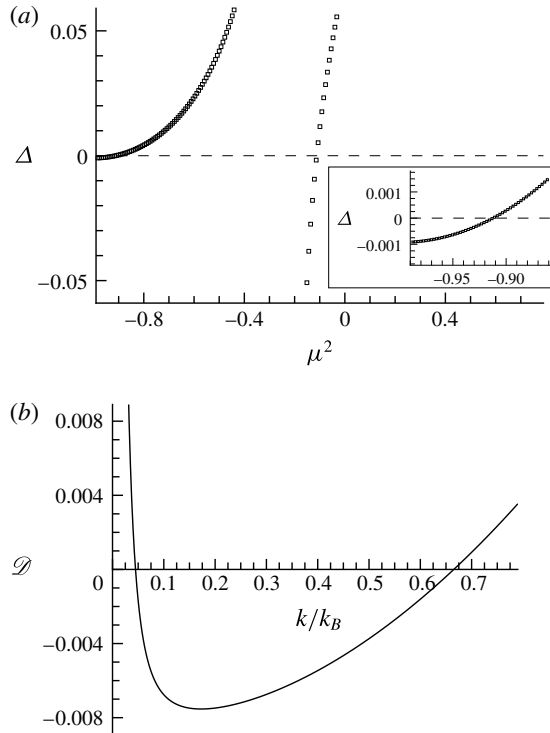


FIGURE 2. (a) Graph of  $\Delta(\sigma, \mu)$  versus  $\mu^2$  for  $\sigma=0.04$  with  $\Delta h_b=0$ . The inset gives the close up for  $-1 < \mu^2 < -0.85$ , showing the root.  $\square$ :  $\text{real}(\Delta)$ ;  $---$ :  $\text{imag}(\Delta)$ . (b) Lamb's dispersion function  $\mathcal{D}(\sigma, \mu_f)$  versus  $\mu_f = k/k_B$  for  $\sigma = 0.04$ . Parameters are  $h_\ell = 0.5$ ,  $h_u = 0.3$ ,  $R = 1.02$ .

equation (A 4) is quadratic in  $\omega^2$ . For a given frequency, it has two wavenumbers: one for the internal mode where the interfacial and free-surface waves are out of phase, and the other for the surface mode (much smaller  $k$ , hence longer wavelength) where the two waves are in phase. In figure 2(a), determinant  $\Delta(\sigma, \mu)$  is plotted as a function of  $\mu^2$  (covering the range for real and imaginary  $\mu$ ) for  $\Delta h_b = 0$ , showing the two roots for  $\sigma = 0.04$ , given  $h_\ell = 0.5$ ,  $h_u = 0.3$  and  $R = 1.02$ . The root  $\mu = 0.3347i$  ( $\mu^2 = -0.1120$ ) gives the internal mode and the other  $\mu = 0.9552i$  ( $\mu^2 = -0.9123$ ) gives the surface mode; see the corresponding waveforms in figure 5. The periodic factor  $P(\xi, \eta; \sigma, \mu)$  is  $2\pi$ -periodic (for an odd- $n$  representation) and reduces to a simple harmonic function as  $\Delta h_b \rightarrow 0$ . Thus, for purely imaginary  $\mu = i\nu$ , the wavenumber given by the Floquet solution is  $k/k_B = 1 - \nu$ . For  $\sigma = 0.04$ , Lamb's equation (A 4) gives  $k/k_B = 0.6653$  ( $= 1 - 0.3347$ ) and  $k/k_B = 0.0448$  ( $= 1 - 0.9552$ ), cf. figure 2(b), confirming the results given by the Floquet solution.

With a sinusoidal bottom  $h_b/h_\ell = 0.6 \cos 2x$  ( $\Delta h_b = 1.2h_\ell$ ), we solve (2.52) and get  $\mu = 0.2947i$  ( $\mu^2 = -0.0869$ ) and  $\mu = 0.9513i$  ( $\mu^2 = -0.9049$ ) for  $\sigma = 0.04$ , keeping other parameters the same; see figure 3(a). The decrease of  $\nu$ , hence the decrease of wavelength (cf. figures 5 and 6), reflects the fact that the effective water depth of the lower layer is reduced due to the presence of bottom topography, being  $h = 0.3819$  in the mapped plane compared with the mean depth  $h_\ell = 0.5$  in the physical plane.

For internal modes, the free-surface displacement is much smaller compared with that at the interface. When the focus is on internal waves, it is common to make

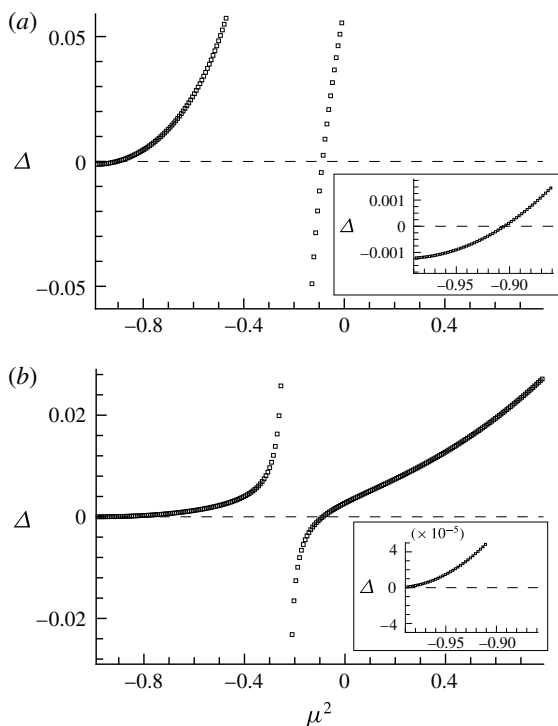


FIGURE 3. Graphs of  $\Delta(\sigma, \mu)$  versus  $\mu^2$  for  $\sigma = 0.04$  and a sinusoidal bottom with height  $\Delta h_b = 1.2h_\ell$ .  $\square$ :  $\text{real}(\Delta)$ ;  $---$ :  $\text{imag}(\Delta)$ . (a) Full calculation of  $\mathbf{M}$  as defined in (2.51); (b) with the rigid-lid approximation. Parameters are  $h_\ell = 0.5$ ,  $h_u = 0.3$ ,  $R = 1.02$ .

the rigid-lid approximation, assuming  $\zeta_u \equiv 0$ , hence suppressing the surface mode. The formulation in §2 can be modified to incorporate the rigid-lid assumption; see appendix B. The calculation of the dispersion relation using (B 3) and (B 5) is shown in figure 3(b). It is seen that the internal mode is retained,  $\mu = 0.2968i$  ( $\mu^2 = -0.0881$ ) for  $\sigma = 0.04$ , and compares well with the full calculation in figure 3(a), while the root for the surface mode disappears.

In the case of a flat bottom, the length scale of the medium in which waves propagate is indefinite. Thus, a wave with arbitrary wavelength (horizontal distance between two adjacent wave crests or troughs) is possible – this manifests the one-to-one relationship between wavenumber  $k$  and  $\omega$  in the case of surface waves in a one-layer homogeneous fluid, and the relation between one  $k$  and two  $\omega$ 's in the case of two-layer fluids (one  $\omega$  for the surface mode and the other for the internal mode). With a periodic seabed, the spatial periodicity of the bottom sets an intrinsic length scale for the wave motion. If the water wavelength is not an integer multiple of the bottom period, the two adjacent wave crests (or troughs) cannot be identical as they see different parts of the topography; therefore the wave must modulate (i.e. slowly vary) in space. When the frequency is outside the forbidden bands, the Floquet exponent is imaginary,  $\mu = i\nu$ , and the wave becomes quasi-periodic, with its amplitude oscillating in space. (These are analogous to Bloch waves in a crystal which can exist in an open domain of continuous periodic medium.) If  $\nu$  is a rational number, the wave field can exactly repeat itself over an integer number of wavelengths, giving a spatially periodic fluid motion. Waves with wavelength

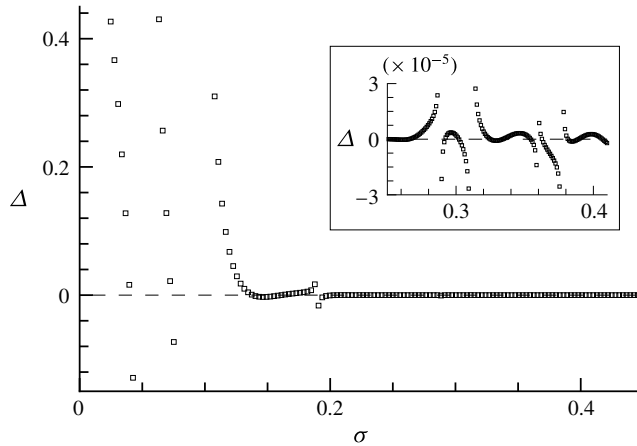


FIGURE 4. Graph of  $\Delta(\sigma, \mu)$  versus  $\sigma$  for  $\mu = 0.2947i$  over the sinusoidal bottom with  $\Delta h_b = 1.2h_\ell$ . The inset gives close up for  $0.25 < \sigma < 0.4$ , showing the multiple roots.  $\square$ :  $\text{real}(\Delta)$ ;  $---$ :  $\text{imag}(\Delta)$ . Parameters are  $h_\ell = 0.5$ ,  $h_u = 0.3$ ,  $R = 1.02$ .

shorter than the bottom wavelength must always modulate. The longer the water wavelength is, the greater the modulation length is, hence the weaker the amplitude variation becomes. Periodic waves, with identical adjacent crests and troughs, occur when  $\mu = (1 - 2/m)i$ , where integer  $m > 2$ , having wavelengths  $\lambda = m\lambda_{bed}$ . Bragg resonances occur when  $\lambda \simeq (2/m')\lambda_{bed}$ ,  $m' = 1, 2, \dots$

Adding an integer to the imaginary part of  $\mu$  is equivalent to shifting the index  $n$  in the Fourier series of the periodic factor  $P$ , effectively changing the period of the dominating Fourier components. This means that given a value of  $\mu$ , we expect to find more than two  $\sigma$ 's that satisfy the dispersion relation (2.52), including short waves that can fit into, or modulate in, the length corresponding to  $\mu$ . This is seen in figure 4 for  $\mu = 0.2947i$  over the sinusoidal bottom. The first root  $\sigma = 0.04$  is the internal mode (wavelength close to  $3\pi$ ) seen in figure 3(a); the second and third roots  $\sigma = 0.0729, 0.1383$  correspond, respectively, to the internal modes of wavelengths slightly shorter than  $2\pi$  and  $\pi$ , having the same modulation length, followed by more roots for even shorter waves. For the convenience of interpreting results, it seems to be better to choose a frequency  $\sigma$ , finding  $\mu$ , as in figure 3.

#### 4. The waveforms

Once the dispersion relation (2.52) is solved, the vector in the null space of  $\mathbf{M}$  gives the solution for  $D_n$ , and  $B_n$  which follows from (2.50). At the interface, the waveform is written from (2.18) as

$$\hat{\zeta}_\ell(x) = i\sigma^{-1} \hat{\phi}_{u,z}|_{z=0} = i\sigma^{-1} \sum_{n=-\infty}^{\infty} e^{(\mu+in)x} B_n Y_n. \quad (4.1)$$

From the normalized (2.7), the waveform at the free surface is

$$\hat{\zeta}_u(x) = i\sigma^{-1} \hat{\phi}_{u,z}|_{z=h_u} = i\sigma \sum_{n=-\infty}^{\infty} e^{(\mu+in)x} \frac{B_n}{\cosh[(n-i\mu)h_u]}. \quad (4.2)$$

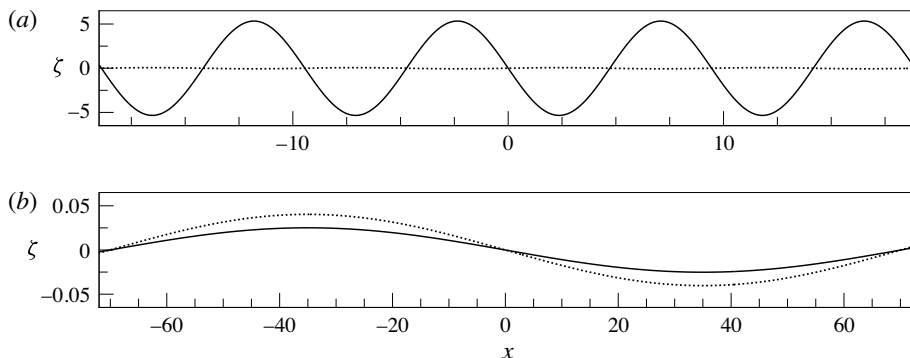


FIGURE 5. Waveforms at  $t=0$  for  $\Delta h_b=0$  (flat bed). —:  $\zeta_\ell$ ;  $\cdots$ :  $\zeta_u$ . (a) Internal mode:  $\sigma=0.04$ ,  $\mu=0.3347i$ . (b) Surface mode:  $\sigma=0.04$ ,  $\mu=0.9552i$ . Parameters are  $h_\ell=0.5$ ,  $h_u=0.3$ ,  $R=1.02$ .

We first check the calculation of (4.1) and (4.2) against the known results for a flat bottom (Lamb 1932), by setting  $\Delta h_b=0$ . For the two roots in figure 2(a), the waveforms are shown in figure 5. For the internal mode,  $\zeta_u$  and  $\zeta_\ell$  are out of phase, with an amplitude ratio  $a_u/a_\ell=0.0121$ ; for the surface mode,  $\zeta_u$  and  $\zeta_\ell$  are in phase, with  $a_u/a_\ell=1.6047$ . These exactly agree with Lamb's results, cf. (A 5).

Over the sinusoidal bottom,  $\zeta_\ell$  of the internal mode becomes less sinusoidal in  $x$ , clearly modulating at the scale comparable to the wavelength, whereas  $\zeta_\ell$  of the surface mode becomes a long wave with short waves riding on it; see figure 6. These short waves have a wavelength  $\pi$ , equal to that of the bottom. They are stationary relative to the long wave. Their amplitudes are comparable to that of the long wave, modulating along it and vanishing at the long wave crests and troughs. An example for a more complex and less smooth bottom profile is shown in figure 7. It is interesting to note that the short waves become out of phase passing a long wave crest or trough. These short waves are not simply copies, or rescaled versions, of the bottom shapes. This is clear from the nonlinear dependence on the Jacobian of transformation  $J$  in the boundary condition at the interface, cf. (2.30).

The presence of short waves in  $\zeta_\ell$  of a surface mode is a striking new feature, and can be understood by examining the case of small bottom amplitude, denoted by  $\epsilon_b$ . When  $\epsilon_b \ll 1$ , we can solve the lower-layer problem in the  $(x, z)$  plane, seeking for the perturbation solution  $\hat{\phi}_\ell = \hat{\phi}_{\ell 0} + \epsilon_b \hat{\phi}_{\ell 1} + \cdots$ . The boundary condition (2.16) at the seabed can be approximated using the Taylor expansion at  $z=-h_\ell$ , yielding

$$\hat{\phi}_{\ell 0, z} = 0 \quad \text{at } z = -h_\ell, \quad (4.3)$$

$$\hat{\phi}_{\ell 1, z} = h_{b, x} \hat{\phi}_{\ell 0, x} - h_b \hat{\phi}_{\ell 0, zz} \quad \text{at } z = -h_\ell. \quad (4.4)$$

The leading-order solution is that of a two-layer fluid over a flat bottom, i.e. the free wave  $\phi_{\ell 0} \sim e^{i(\mu_f x - \sigma t)}$ , where  $\mu_f = k/k_B \ll 1$  for the surface mode and satisfies Lamb's dispersion relation (A 4). At the next order, we have a forced problem, with  $\hat{\phi}_{\ell 1}$  being generated due to the interaction of  $\phi_{\ell 0}$  and bottom  $h_b(x) \sim e^{i2x} + \text{c.c.}$  (Effects due to nonlinear convective inertia are not considered.) It follows from (4.4) that  $\hat{\phi}_{\ell 1}$  must consist of harmonics  $e^{i(\mu_f+2)x}$ ,  $e^{i(\mu_f-2)x}$  and their complex conjugates. This leads to a waveform  $\zeta_\ell \sim [a_0 + \epsilon_b(a_1 e^{i2x} + b_1 e^{-i2x})] e^{i(\mu_f x - \sigma t)} + \text{c.c.}$ , explaining the short wave

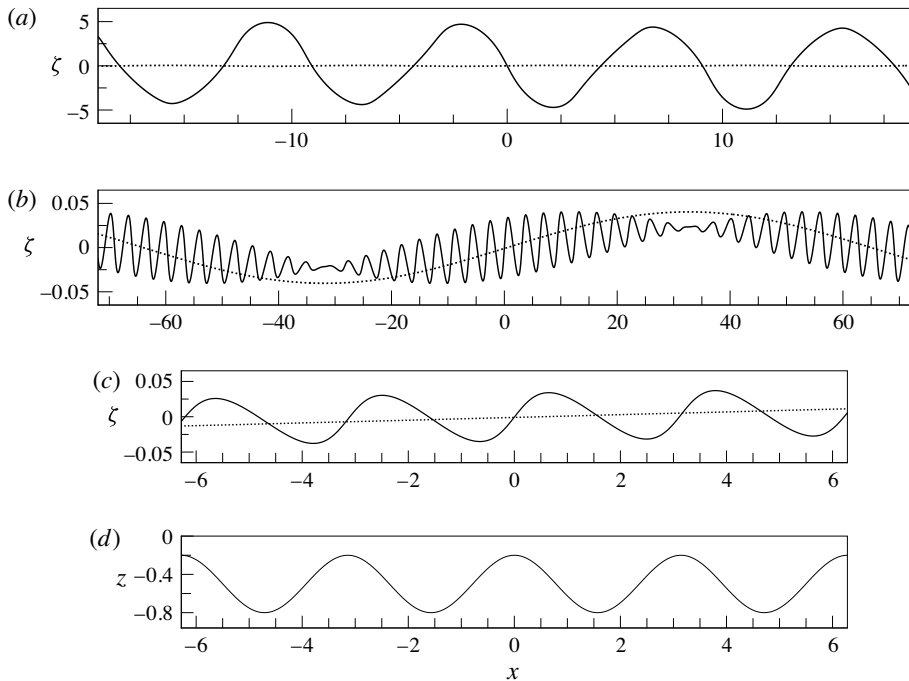


FIGURE 6. Waveforms at  $t = 0$  over the sinusoidal bottom with  $\Delta h_b = 1.2h_\ell$  for  $\sigma = 0.04$ . —:  $\zeta_\ell$ ;  $\cdots$ :  $\zeta_u$ . (a) Internal mode:  $\mu = 0.2947i$ . (b) Surface mode:  $\mu = 0.9513i$ . Parameters are  $h_\ell = 0.5$ ,  $h_u = 0.3$ ,  $R = 1.02$ . (c) A section of graph (b) in  $-6.28 < x < 6.28$ , comparing the short wavelength variations in  $\zeta_\ell$  with the bottom profile in (d):  $h_b/h_\ell = 0.6 \cos 2x$ . The undisturbed interface is at  $z = 0$ .

variations at the scale of the bottom wavelength. The amplitude modulation and phase changes of short waves are due to the dependence on the derivatives of  $\hat{\phi}_{\ell 0}$ . For large-amplitude bottoms, this essential physics of fluid–bottom interaction remains, but the short waves are no longer simple harmonics in  $x$  but general periodic functions.

When the frequencies are inside the forbidden bands, the internal modes are strongly affected by the bottom due to Bragg resonance. For the internal mode, the resonant interfacial wave  $\zeta_\ell$  has an amplitude that grows exponentially in  $x$  (or decay in  $-x$ , as  $\pm\mu$  are now real), whereas for the surface mode, the amplitude of short waves can exceed that of the long wave carrier. figure 8 shows the resonant interfacial waves with wavelengths close to  $2\pi$  and  $2\pi/3$  (i.e. the primary  $m = 1$  and tertiary  $m = 3$  Bragg reflections), and the corresponding surface modes.

In the examples above, the waveforms  $\zeta_u$  of the surface modes are virtually unaffected. The short wave variations in  $\zeta_\ell$ , though having amplitudes comparable to the long wave carrier, are nevertheless of small amplitude because of the linear wave theory. (They are of course also small because the surface displacement of the surface mode, and hence its interface displacement, is much smaller than the interface displacement due to the internal mode.) Thus, the short waves in  $\zeta_\ell$  are not much felt by the long waves at the upper surface. However, when the surface modes have wavelengths comparable to that of the bottom,  $\zeta_u$  can be noticeably affected, since the interface is seen by  $\zeta_u$  to be sufficiently ‘rough’.

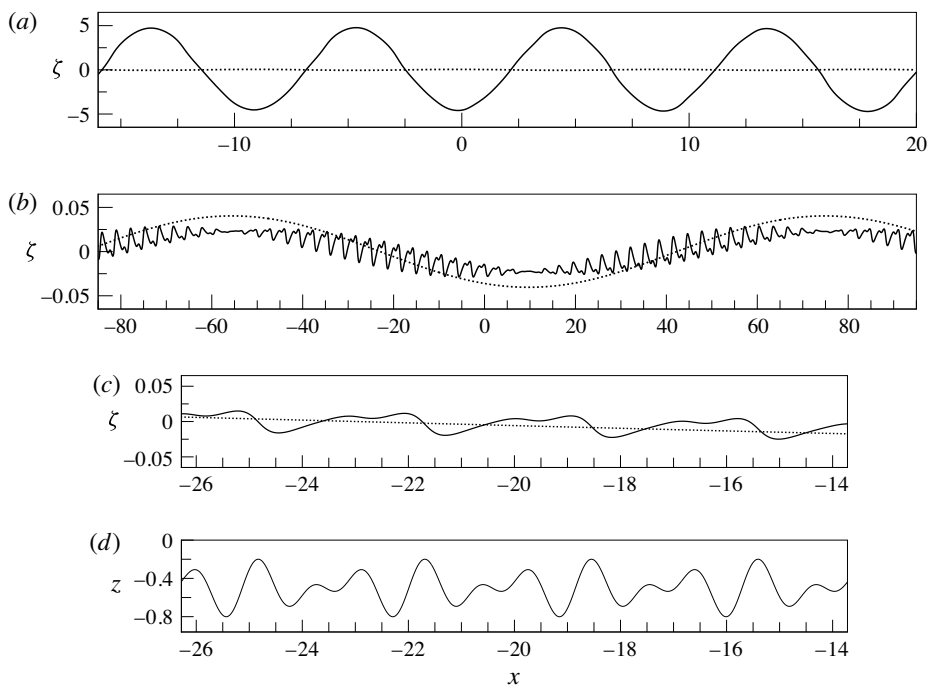


FIGURE 7. Waveforms at  $t=0$  over a doubly sinusoidal bottom for  $\sigma = 0.04$ . —:  $\zeta_\ell$ ; ·····:  $\zeta_u$ . (a) Internal mode:  $\mu = 0.3023i$ . (b) Surface mode:  $\mu = 0.9518i$ . Parameters are  $h_\ell = 0.5$ ,  $h_u = 0.3$ ,  $R = 1.02$ . (c) A section of graph (b) in  $-26.28 < x < -13.72$ , comparing the short wavelength variation in  $\zeta_\ell$  with the bottom profile in (d):  $h_b/h_\ell = 0.3154(\sin 4x + \sin 6x)$ , i.e.  $\Delta h_b = 1.20h_\ell$ . The undisturbed interface is at  $z=0$ .

While the presence of small amplitude, ‘fast’ (short scale) variations at the interface due to a long surface wave may have gone unnoticed, the gradient due to the short-scale waves and the associated velocity field, are much larger than those due to the carrier long wave. And necessarily so, as the velocity field is forced to respond at the scale at which the topographic variations occur. All this is particularly relevant in shallow seas, where the top and bottom layers are mixed by winds and tides, respectively, and the density interface (pycnocline) often is close to the bottom. In the deep ocean, however, the bottom layer is much thicker and the influence of bed corrugations may not be strongly felt at the pycnocline, and the short-scale variations are thus lacking in that case.

## 5. Future challenges

The consideration of linear waves over a periodic bottom undulation, of arbitrary amplitude and shape but fully submerged in the lower layer of a two-layer fluid, is a first step towards bridging the gap with the linear, 2-D internal waves arising in continuously stratified fluids confined to enclosed domains. In applying this work to a confined, continuously stratified sea, the present two-layer problem requires modification by adding (1) vertical sidewalls, as for the surface wave problem in Howard & Yu (2007) and Weidman *et al.* (2015), (2) slopes to these sidewalls and (3) multiple layers. Three comments can be made regarding these additions.



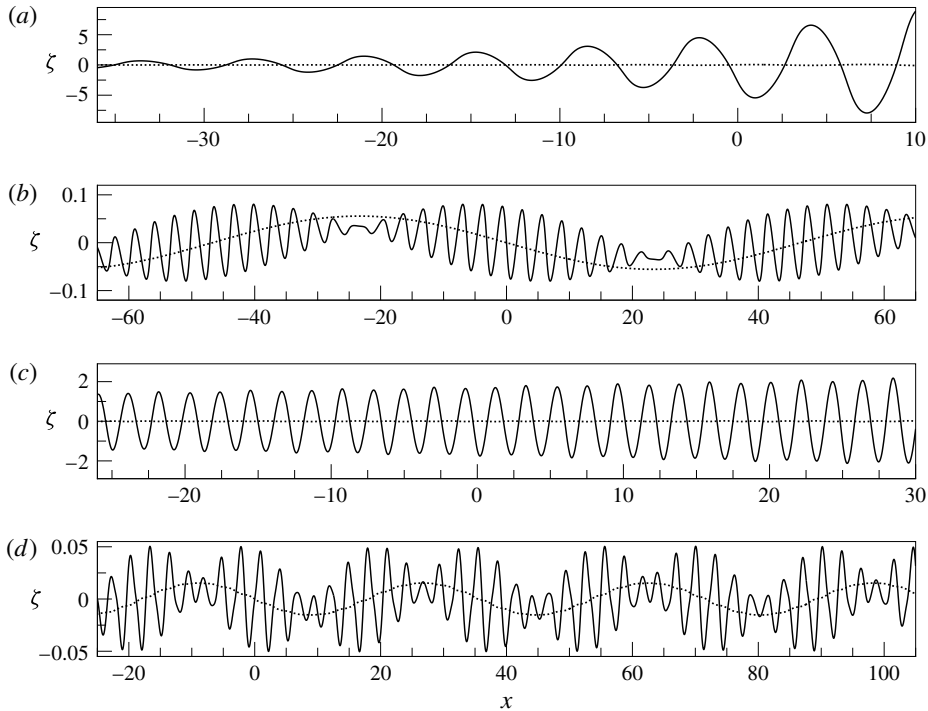


FIGURE 8. Resonant waveforms at  $t = 0$  over the sinusoidal bottom with  $\Delta h_b = 1.2h_\ell$ . —:  $\zeta_\ell$ ; ·····:  $\zeta_u$ . For  $\sigma = 0.055$  ( $\lambda$  close to  $2\pi$ , i.e. the primary  $m = 1$  resonance): (a) internal mode,  $\mu = 0.0603$ ; (b) surface mode,  $\mu = 0.9328i$ . For  $\sigma = 0.15$  ( $\lambda$  close to  $2\pi/3$ , i.e. the tertiary  $m = 3$  resonance): (c) internal mode,  $\mu = 0.0076$ ; (d) surface mode,  $\mu = 0.8242i$ . Parameters are  $h_\ell = 0.5$ ,  $h_u = 0.3$ ,  $R = 1.02$ .

First, the addition of a sloping side wall has been solved for surface waves in an infinite wedge (see Whitham (1979)). Application to confined fluid domains is, even for the surface wave problem, non-trivial. It requires finding an appropriate combination of wave and evanescent modes (which together constitute a complete basis and are provided by Yu & Howard (2012) for a generally periodic bed), such that the impermeability at the side walls (lateral boundaries) can be satisfied (Weidman *et al.* 2015). Before addressing this issue in layered systems, the existence of a similar, complete basis needs to be investigated. So far, this has not even been discussed for the two-layer case.

Second, in a confined basin, the surface wave spectrum is discrete, while in continuously stratified fluids, the internal wave spectrum is continuous. This transition is brought about by a proliferation of internal wave modes upon increase of the number of layers.

Third, sloping walls provide a coupling between these modes. One needs to find out how interfacial displacements of these modes (i.e. modal amplitudes) organize such as to progressively mimic the oblique propagation of internal waves when increasing the number of layers. This paves the way for discussion of internal wave attractors in multi-layer systems. Internal wave localization on so-called wave attractors occurs in continuously stratified fluids that are confined to containers possessing one or more sloping boundaries (Maas & Lam 1995). Internal waves of frequency less

than the fluid's stability frequency approach these attractors regardless of where they are forced, and, because of geometric focusing, amplify until checked by viscous damping (Hazewinkel *et al.* 2008) or nonlinearity (Scolan, Ermanyuk & Dauxios 2013). Localization of internal waves has been confirmed in laboratory experiments (Maas *et al.* 1997; Hazewinkel *et al.* 2010; Hazewinkel, Grisouard & Dalziel 2011) and numerical experiments (Drijfhout & Maas 2007; Grisouard, Staquet & Pairaud 2008; Echeverri *et al.* 2011).

The mapping method presented in this study requires the bed corrugations to remain in the bottom layer. This could set a limitation to the maximum corrugation height, when extending to multiple layers. On the other hand, in our formulation, the layer thickness is independent, as well as the density within each layer. This can be manipulated to advantage, offsetting the limitation just mentioned and effectively dealing with various density profiles. Still it remains a limitation, in particular in the case of uniformly stratified fluids or, if the number of layers below the pycnocline (assuming it sits above the bottom topography) is important.

### Acknowledgement

This work was first inspired by conversations with R. Camassa. Supports to J.Y. by US National Science Foundation (Grant CBET-0845957) and a visitor's grant of the Netherlands Organisation for Scientific Research (NWO) during the period of this work, are gratefully acknowledged.

### Appendix A. The flat-bottom limit

In the limit  $\Delta h_b \rightarrow 0$ , i.e.  $h_b = 0$ ,  $b_j = c_j = 0$  and  $h = h_\ell$ . It follows from (2.34) that  $f(\xi) = 0$  and  $x = \xi$ . From (2.41),  $A_{n,0} = 1$  and  $A_{n,j} = 0$  for  $j = \pm 1, \pm 2, \dots$ . From (2.29),  $Q = 1$ , hence  $Q_0 = 1$  and  $Q_j = 0$  for  $j = \pm 1, \pm 2, \dots$ , following (2.44). Equations (2.45) and (2.47) reduce to

$$D_n = B_n \left\{ 1 - \left[ \frac{\sigma^2 R^{-1}}{(n - i\mu)} + (1 - R^{-1}) \frac{(n - i\mu)}{\sigma^2} \right] \tanh[(n - i\mu)h_u] \right\}, \quad (\text{A } 1)$$

$$D_n(n - i\mu) \tanh[(n - i\mu)h] = B_n \{ \sigma^2 - (n - i\mu) \tanh[(n - i\mu)h_u] \}. \quad (\text{A } 2)$$

Clearly,  $D_n$  and  $D_{n'}$  are not coupled, nor are  $B_n$  and  $B_{n'}$  for  $n \neq n'$ . Thus, we can set  $D_n = B_n = 0$ , for  $n \neq -1$ , looking for a non-trivial solution with just one term. For  $\mu = i\nu$ , let us write  $1 - \nu = \mu_f$ . From (A 1) and (A 2), for  $n = -1$  we obtain

$$\begin{aligned} & \sigma^2 - \mu_f \tanh(\mu_f h_u) \\ &= \left\{ 1 - \left[ \frac{\sigma^2}{R\mu_f} + (1 - R^{-1}) \frac{\mu_f}{\sigma^2} \right] \tanh(\mu_f h_u) \right\} \mu_f \tanh(\mu_f h_\ell). \end{aligned} \quad (\text{A } 3)$$

After some algebra, it can be rewritten as

$$\begin{aligned} & \sigma^4 [R \coth(\mu_f h_\ell) \coth(\mu_f h_u) + 1] \\ & - \sigma^2 R \mu_f [\coth(\mu_f h_u) + \coth(\mu_f h_\ell)] + (R - 1) \mu_f^2 = 0. \end{aligned} \quad (\text{A } 4)$$

This is Lamb's dispersion relation for two-layer fluids over a flat bottom, written using  $\mu_f = k/k_B$  and  $\sigma = \omega/\sqrt{gk_B}$  by adapting the normalization in the present study. Denoting the left-hand side by  $\mathcal{D}$ , we write (A 4) as  $\mathcal{D}(\sigma, \mu_f, h_u, h_\ell, R) = 0$ . For simple

sinusoidal waves over a flat bottom, (Lamb 1932) also gave the ratio of amplitudes of the displacements of the upper and lower surface rewritten here in dimensionless form as

$$\frac{a_u}{a_\ell} = \frac{1}{\cosh(\mu_f h_u) - \mu_f \sigma^{-2} \sinh(\mu_f h_u)}. \quad (\text{A } 5)$$

## Appendix B. The rigid-lid approximation

Suppose the displacement of the free (upper) surface is negligible, i.e.  $\hat{\zeta}_u \equiv 0$ . The appropriate boundary condition is

$$\hat{\phi}_{u,z} = 0 \quad \text{at } z = h_u. \quad (\text{B } 1)$$

The matching conditions at the interface  $z=0$  remain unchanged, cf. (2.17) and (2.18). Instead of (2.35), the solution for the upper-layer problem, that satisfies the Laplace equation (2.13) and condition (B 1), can now be written as

$$\hat{\phi}_u = \sum_{n=-\infty}^{\infty} e^{(\mu+in)x} \frac{B_n}{\cosh[(n-i\mu)h_u]} \cosh[(n-i\mu)(z-h_u)]. \quad (\text{B } 2)$$

Using this solution, we redo the matching conditions at  $z=0$ , following the algebra in (2.3). The pressure condition (2.17) leads to

$$R \sum_{j=-\infty}^{\infty} D_{n-2j} A_{n-2j,j} = B_n \tilde{L}_n(\sigma, \mu), \quad (\text{B } 3)$$

where

$$\tilde{L}_n(\sigma, \mu) = 1 - (R-1) \frac{(n-i\mu)}{\sigma^2} \tanh[(n-i\mu)h_u]. \quad (\text{B } 4)$$

The kinematic condition (2.18) gives

$$\sum_{j=-\infty}^{\infty} D_{n-2j} A_{n-2j,j} Z_{n-2j}(\mu) = \sum_{j=-\infty}^{\infty} B_{n-2j} Q_j \tilde{Y}_{n-2j}(\mu), \quad (\text{B } 5)$$

where

$$\tilde{Y}_n(\mu) = -(n-i\mu) \tanh[(n-i\mu)h_u]. \quad (\text{B } 6)$$

Equations (B 3) and (B 5) replace (2.45) and (2.47), determining the dispersion relationship between  $\sigma$  and  $\mu$  under the assumption of a rigid lid. From (2.37) and (2.39), for  $\sigma \ll 1$  and fixed  $n$ ,  $L_n(\sigma, \mu) = \tilde{L}_n(\sigma, \mu) + O(\sigma^2)$  and  $Y_n(\sigma, \mu) = \tilde{Y}_n(\mu) + O(\sigma^2)$ .

## REFERENCES

- ALAM, M.-R., LIU, Y. & YUE, D. K. P. 2009 Bragg resonance of waves in a two-layer fluid propagating over bottom ripples. Part I. Perturbation analysis. *J. Fluid Mech.* **624**, 191–224.
- ATHANASSOULIS, G. A. & BELIBASSAKIS, K. A. 1999 A consistent coupled-mode theory for the propagation of small-amplitude water waves over variable bathymetry regions. *J. Fluid Mech.* **389**, 275–301.

- DRIJFHOUT, S. & MAAS, L. R. M. 2007 Impact of channel geometry and rotation on the trapping of internal tides. *J. Phys. Oceanogr.* **37**, 2740–2763.
- ECHEVERRI, P., YOKOSHI, T., BALMFORTH, N. J. & PEACOCK, T. 2011 Tidally generated internal-wave attractors between double ridges. *J. Fluid Mech.* **669**, 354–374.
- GRISOUD, N., STAQUET, C. & PAIRAUD, I. 2008 Numerical simulation of a two-dimensional internal wave attractor. *J. Fluid Mech.* **614**, 1–14.
- HAZEWINKEL, J., VAN BREEVOORT, P., DALZIEL, S. B. & MAAS, L. R. M. 2008 Observations on the wavenumber spectrum and evolution of an internal wave attractor. *J. Fluid Mech.* **598**, 373–382.
- HAZEWINKEL, J., GRISOUD, N. & DALZIEL, S. B. 2011 Comparison of laboratory and numerically observed scalar fields of an internal wave attractor. *Eur. J. Mech. (B/Fluids)* **30** (1), 51–56.
- HAZEWINKEL, J., TSIMITRI, C., MAAS, L. R. M. & DALZIEL, S. B. 2010 Observations on the robustness of internal wave attractors to perturbations. *Phys. Fluids* **22**, 107102.
- HOWARD, L. N. & YU, J. 2007 Normal modes of a rectangular tank with corrugated bottom. *J. Fluid Mech.* **593**, 209–234.
- LAMB, H. 1932 *Hydrodynamics*. Cambridge University Press.
- LIU, Y. & YUE, D. K. P. 1998 On generalised Bragg scattering of surface waves by bottom ripples. *J. Fluid Mech.* **356**, 297–326.
- MAAS, L. R. M., BENIELLI, D., SOMMERIA, J. & LAM, F.-P. A. 1997 Observation of an internal wave attractor in a confined stably-stratified fluid. *Nature* **388**, 557–561.
- MAAS, L. R. M. & LAM, F.-P. A. 1995 Geometric focusing of internal waves. *J. Fluid Mech.* **300**, 1–41.
- PIETRZAK, J. D., KRANENBURG, C. & ABRAHAM, G. 1990 Resonant internal waves in fluid flow. *Nature* **344**, 844–847.
- PIETRZAK, J. D. & LABEUR, R. J. 2004 Trapped internal waves over undular topography in a partially mixed estuary. *Ocean. Dyn.* **54**, 315–323.
- RHINES, P. & BRETHERTON, F. 1973 Topographic Rossby waves in a rough-bottomed ocean. *J. Fluid Mech.* **61**, 583–607.
- SCOLAN, H., ERMANYUK, E. & DAUXIOS, T. 2013 Nonlinear fate of internal wave attractors. *Phys. Rev. Lett.* **110** (23), 234501.
- WEIDMAN, P. D., HERCZYNSKI, A., YU, J. & HOWARD, L. N. 2015 Experiments on standing waves in a rectangular tank with a corrugated bed. *J. Fluid Mech.* **777**, 122–150.
- WHITHAM, G. B. 1979 *Lectures on Wave Propagation*. Published for the Tata Institute of Fundamental Research, Springer.
- YU, J. & HOWARD, L. N. 2010 On higher order Bragg resonance of water waves by bottom corrugations. *J. Fluid Mech.* **659**, 484–504.
- YU, J. & HOWARD, L. N. 2012 Exact Floquet theory for waves over arbitrary periodic topographies. *J. Fluid Mech.* **712**, 451–470.
- YU, J. & ZHENG, G. 2012 Exact solutions for wave propagation over a patch of large bottom corrugations. *J. Fluid Mech.* **713**, 362–375.